Journal of Engineering Mathematics (2005) 52: 185–198
DOI 10.1007/s10665-004-1771-8


# Large-strain dynamic cavity expansion in a granular material

V.A. OSINOV
*Institute for Geotechnical Engineering, University of Natural Resources and Applied Life Sciences, Feistmantelstr. 4, A-1180 Vienna, Austria (vladimir.osinov@boku.ac.at)*

Received 20 June 2004; accepted in revised form 26 July 2004

**Abstract.** The dynamic problem of the symmetric expansion of a cylindrical or spherical cavity in a granular medium is considered. The constitutive behaviour of the material is governed by a hypoplasticity relation for granular soils capable of describing both monotonic and cyclic deformation. The problem is solved numerically by a finite-difference technique. A nonreflecting boundary condition used at the outer boundary of the computational domain makes it possible to model a continuous multi-cycle loading on the cavity wall. The solution is illustrated by numerical examples. Possible geomechanical applications to the modelling of the vibratory compaction and penetration in granular soils are discussed.

**Key words:** dynamic cavity expansion, granular material, hypoplasticity, transparent boundary condition

## 1. Introduction

The present paper is devoted to the numerical solution of the dynamic problem of the symmetric expansion of a cylindrical or spherical cavity in a granular medium. The study is orientated towards geomechanical applications. The cavity-expansion problem is widely used in geomechanics for the modelling of various processes (*e.g.* penetration) in soils and rocks [1]. As far as granular soils are concerned, most analyses of the cavity-expansion problem are carried out for the quasi-static monotonic expansion in order to determine the limit pressure and/or the pressure-expansion curve [2–7].

For the modelling of processes in which the rate of loading is high, the use of a quasi-static formulation of the cavity problem is inadequate, and a dynamic formulation is necessary. The difference between the quasi-static and the dynamic solutions may be substantial. For instance, for a cylindrical cavity in a linear elastic medium, the stresses in the quasi-static problem vary as $1/r^2$, while in the dynamic problem the stresses decay asymptotically for $r \to \infty$ as $1/\sqrt{r}$.

In the geotechnical context, it is clear intuitively that the modelling of such processes as vibratory pile driving or deep vibratory compaction (also called vibroflotation [8]) requires a dynamic formulation. However, because of the nonlinear behaviour of soils at large deformations, it may be difficult to make a quantitatively justified *a priori* judgement about the necessity of using the dynamic formulation for a particular problem. In the case of the cavity problem with a periodic boundary condition, a quantitative criterion for using the dynamic formulation is that the wavelength for a given frequency is of the same order as or smaller than the cavity diameter. The difficulty in using this criterion consists in the fact that the incremental stiffness of a soil changes considerably during large plastic deformation. The speed of propagation of small-amplitude elastic waves, which is often known for a particular soil, is not applicable to the estimation of the wavelength when the large-strain expansion of a cavity is studied: the wave speed corresponding to the incremental stiffness may be much

lower and, moreover, hardly predictable as it depends on the strain. In such cases the necessity of using a dynamic formulation can only be justified after the solutions to the dynamic problem have been obtained. This issue is discussed in more detail below in Section 5 where numerical examples are considered.

In this paper we solve the dynamic problem allowing for the possibility of prescribing a multi-cycle loading on the cavity wall expressed either through the cavity pressure or the cavity radius. Unlike problems with a monotonic or single-cycle loading, the cavity expansion problem with a multi-cycle boundary condition requires the use of a proper constitutive model which realistically describes the behaviour of a granular material under repeated loading and, in particular, its gradual compaction under cyclic shearing. In this study we employ an extended constitutive relation of the hypoplasticity theory developed in [9] and capable of describing both monotonic and cyclic deformation of granular materials such as sand. This hypoplasticity relation was used earlier in [10–12] for the numerical solution of dynamic plan-wave problems for granular soils. A number of particular solutions to the dynamic-cavity problem with a simple version of the hypoplasticity relation were obtained in [13].

The constitutive theory used in the present study is outlined in Section 2. The mathematical formulation of the initial-boundary-value problem is described in Section 3. The problem is solved numerically by a finite-difference technique described in Section 4. Numerical examples are given in Section 5, and possible geotechnical applications are briefly discussed at the end of the paper.

## 2. Hypoplasticity relations

The theory of hypoplasticity originated as an alternative to elasto-plasticity theories for the purpose of describing the plastic deformation of granular materials without the introduction of a yield surface, a flow rule and without the decomposition of the deformation into an elastic and a plastic part. Attempts to find a suitable mathematical form including the pressure and density dependence of the stiffness had led to an equation written in rectangular coordinates as [14, 15]

$$\frac{\mathrm{d}T_{ij}}{\mathrm{d}t} = \mathcal{L}_{ijkl}(\mathbf{T}, e) D_{kl} + N_{ij}(\mathbf{T}, e)\|\mathbf{D}\|, \tag{1}$$

where $\mathbf{T}$ is the Cauchy stress tensor, $\mathbf{D}$ is the stretching tensor (the symmetric part of the velocity gradient), $e$ is the void ratio, $t$ is time, and $\mathrm{d}(\,)/\mathrm{d}t$ stands for the material time derivative (for simplicity, we write the material time derivative instead of an objective stress rate; for the velocity fields considered in this paper the objective Jaumann stress rate used in hypoplasticity coincides with the material time derivative). The fourth-order stiffness tensor $\mathcal{L}$ and the second-order tensor $\mathbf{N}$ in (1) are responsible, respectively, for the linear and the nonlinear parts of the constitutive relation. The term $\|\mathbf{D}\| = \sqrt{D_{ij} D_{ij}}$ makes the constitutive equation incrementally nonlinear. Material parameters involved in a specific form of the tensors $\mathcal{L}$ and $\mathbf{N}$ are independent of the stresses and the density. Equation (1) also allows the critical-state concept to be incorporated into the theory. The tensors $\mathcal{L}$ and $\mathbf{N}$ are given in detail in the Appendix.

A limitation of the hypoplasticity concept expressed in the form (1) is the so-called ratcheting which manifests itself in an unrealistically high rate of accumulation of deformation or stress during repeated multi-cycle loading with small strain amplitudes (below $10^{-2}$) [16, 17]. This is inevitable as long as the state of a granular material and therefore its stiffness are determined only by stresses and density.

In order to better describe the behaviour of granular materials and, in particular, their response to alternating cyclic loading, the concept of intergranular strain was introduced in [9] as an extension of hypoplasticity. This concept as such is not related to a specific hypoplastic equation and is applicable to any equation of the form (1). The extended constitutive theory contains a so-called intergranular-strain tensor $\boldsymbol{\delta}$ as a new state variable which carries the information about the history of the deformation and determines the state of the material along with the stress tensor and the void ratio.

The hypoplasticity relation in the extended form becomes

$$\frac{\mathrm{d}T_{ij}}{\mathrm{d}t} = \mathcal{M}_{ijkl}(\mathbf{T}, \mathbf{D}, \boldsymbol{\delta}, e) D_{kl}, \tag{2}$$

where the tensor $\mathcal{M}$ includes the tensors $\mathcal{L}$ and $\mathbf{N}$ from (1). The intergranular-strain tensor is determined by its evolution equation

$$\frac{\mathrm{d}\delta_{ij}}{\mathrm{d}t} = F_{ij}(\mathbf{D}, \boldsymbol{\delta}). \tag{3}$$

For detailed forms of $\mathcal{M}$ and $\mathbf{F}$, see the Appendix.

The function $\mathbf{F}$ in (3) is such that, under monotonic loading with a fixed direction of deformation $\mathbf{D}/\|\mathbf{D}\|$, the tensor $\boldsymbol{\delta}$ tends asymptotically to a certain value. In turn, the tensor $\mathcal{M}$ is constructed in such a way that, as $\boldsymbol{\delta}$ approaches its asymptotic value, the constitutive response of (2) approaches the response of the basic equation (1). Thus, during monotonic unidirectional deformation the extended equation gradually turns into the original one. On the other hand, for small-amplitude alternating deformation the response produced by (2), (3) is close to being linearly elastic, if the amplitude is small enough.

An initial value of $\boldsymbol{\delta}$ required for the integration of Equation (3) is often indeterminate when solving a particular problem. Note that the indeterminacy of the initial values of certain state variables is typical of plasticity models in which these variables are determined by the foregoing deformation. In problems with multi-cycle deformation, the influence of the initial value of $\boldsymbol{\delta}$ vanishes after 2–3 cycles. In the numerical calculations in this paper the initial value of $\boldsymbol{\delta}$ is taken to be zero.

Examples of how the extended hypoplasticity relation works for cyclic loading can be found in [12].

## 3. Boundary-value problem

In the dynamic problem, constitutive equations (2), (3) are supplemented with the evolution equation for the void ratio (with incompressible grains)

$$\frac{\mathrm{d}e}{\mathrm{d}t} = (1+e)\ \mathrm{tr}\,\mathbf{D} \tag{4}$$

and the equation of motion (without mass forces)

$$\mathrm{div}\,\mathbf{T} = \varrho \frac{\mathrm{d}\mathbf{v}}{\mathrm{d}t}, \tag{5}$$

where $\mathbf{v}$ is the velocity field, and $\varrho$ is the density of the material.

We study the problem of the symmetric expansion of a cavity in which all quantities are functions of the radial coordinate and time. In the cylindrical coordinates $r, \varphi, z$, a symmetric expansion under plane strain conditions (infinitely long cavity) is described by the velocity component $v_r$, the stress components $T_{rr}, T_{\varphi\varphi}, T_{zz}$, the intergranular-strain components

$\delta_{rr}, \delta_{\varphi\varphi}$ and the void ratio $e$. The stretching tensor has two nonzero components $D_{rr} = \partial v_r / \partial r$ and $D_{\varphi\varphi} = v_r / r$. In what follows, for brevity we will write $v, T_r, T_\varphi, T_z, \delta_r, \delta_\varphi$, respectively, for $v_r, T_{rr}, T_{\varphi\varphi}, T_{zz}, \delta_{rr}, \delta_{\varphi\varphi}$.

In cylindrical coordinates, Equations (5), (4) are written, respectively, as

$$\frac{\partial T_r}{\partial r} + \frac{1}{r}(T_r - T_\varphi) = \varrho \frac{\mathrm{d}v_r}{\mathrm{d}t}, \tag{6}$$

$$\frac{\mathrm{d}e}{\mathrm{d}t} = (1+e)\left(\frac{\partial v}{\partial r} + \frac{v}{r}\right). \tag{7}$$

For brevity, we do not write out the constitutive functions in detail; for the considered case of cylindrical symmetry this can easily be done using the functions given in the Appendix. We write the constitutive equations in general form showing only the dependence of the time derivatives on the other functions involved in the problem:

$$\frac{\mathrm{d}T_r}{\mathrm{d}t} = H_r\left(T_r, T_\varphi, T_z, \frac{\partial v}{\partial r}, \frac{v}{r}, \delta_r, \delta_\varphi, e\right), \tag{8}$$

$$\frac{\mathrm{d}T_\varphi}{\mathrm{d}t} = H_\varphi\left(T_r, T_\varphi, T_z, \frac{\partial v}{\partial r}, \frac{v}{r}, \delta_r, \delta_\varphi, e\right), \tag{9}$$

$$\frac{\mathrm{d}T_z}{\mathrm{d}t} = H_z\left(T_r, T_\varphi, T_z, \frac{\partial v}{\partial r}, \frac{v}{r}, \delta_r, \delta_\varphi, e\right), \tag{10}$$

$$\frac{\mathrm{d}\delta_r}{\mathrm{d}t} = F_r\left(\frac{\partial v}{\partial r}, \frac{v}{r}, \delta_r, \delta_\varphi\right), \tag{11}$$

$$\frac{\mathrm{d}\delta_\varphi}{\mathrm{d}t} = F_\varphi\left(\frac{\partial v}{\partial r}, \frac{v}{r}, \delta_r, \delta_\varphi\right). \tag{12}$$

The initial-boundary-value problem for Equations (6–12) with the unknown functions $v, T_r, T_\varphi, T_z, \delta_r, \delta_\varphi, e$ is formulated for a domain $r \in [r_a(t), r_b(t)], t \geqslant 0$, where $r_a(t)$ is the radius of the cavity, and $r_b(t)$ is the outer radius of the domain where the solution is sought. For a cavity in an infinite body, $r_b = \infty$. The motion of the boundaries $r_a(t), r_b(t)$ is determined by the integration of the velocity starting with initial values $r_a^0, r_b^0$. Initial conditions for all the functions are prescribed on the interval $[r_a^0, r_b^0]$.

The boundary condition at $r_a(t)$ and $r_b(t)$ can be taken as either the velocity or the stress component $T_r$ as a function of time. For a cavity in an infinite body it is natural to put $v(\infty) = 0$ or $T_r(\infty) = \text{const}$. However, in the numerical solution an infinite outer radius, as required by the mathematical formulation of the problem, is replaced with a finite radius $r_b$. This leads to a spurious reflection from the outer boundary with either of the conditions $v(\infty) = 0, T_r(\infty) = \text{const}$. Increasing the outer radius does not eliminate this problem: although the amplitude of the outgoing and, correspondingly, the reflected waves may be small and even negligible far away from the cavity owing to geometrical attenuation, the amplitude of the reflected waves increases again as they approach the cavity because of the same geometrical effect. Even in the presence of material damping the reflected waves in the vicinity of the cavity may essentially distort the solution as compared to that for an infinite domain. This fact makes it necessary to introduce a nonreflecting boundary condition at $r_b$ which will make the boundary transparent for outgoing waves and thus imitate an unbounded domain.

Since the amplitude of a wave substantially decreases as it propagates from the cavity, the wave far away from the cavity can be well approximated by a linear elastic wave. If, in addition, we neglect the cylindrical or spherical geometry and assume the wave at $r \gg r_a$ to be a plane longitudinal one, this allows us to prescribe a simple nonreflecting boundary condition at $r_b \gg r_a$. For a plane elastic wave propagating in the positive $x$-direction with a wave speed $c$ and described by a function $f(x-ct)$, the partial derivatives are connected with each other as $\partial f/\partial t = -c\partial f/\partial x$. The required boundary condition in terms of velocity thus takes the form

$$\left.\frac{\partial v}{\partial t}\right|_{(r_b,t)} = -c \left.\frac{\partial v}{\partial r}\right|_{(r_b,t)} \tag{13}$$

with the wave speed $c = \sqrt{C/\varrho}$, where the small-strain uniaxial stiffness $C$ at $r = r_b$ can be found directly from the constitutive equation used. The effectiveness of the boundary condition (13) will be demonstrated later by a numerical example.

For a spherical cavity, the symmetric expansion is described in spherical coordinates $r, \varphi, \theta$ by the velocity component $v_r$, the stress components $T_{rr}, T_{\varphi\varphi} = T_{\theta\theta}$, the intergranular-strain components $\delta_{rr}, \delta_{\varphi\varphi} = \delta_{\theta\theta}$ and the void ratio $e$. The stretching tensor has three nonzero components $D_{rr} = \partial v_r/\partial r$ and $D_{\varphi\varphi} = D_{\theta\theta} = v_r/r$. The equation of motion, the constitutive equations and the mass-balance equation for a spherical cavity are written, respectively, as

$$\frac{\partial T_r}{\partial r} + \frac{2}{r}(T_r - T_\varphi) = \varrho \frac{\mathrm{d}v_r}{\mathrm{d}t}, \tag{14}$$

$$\frac{\mathrm{d}T_r}{\mathrm{d}t} = H_r\left(T_r, T_\varphi, \frac{\partial v}{\partial r}, \frac{v}{r}, \delta_r, \delta_\varphi, e\right), \tag{15}$$

$$\frac{\mathrm{d}T_\varphi}{\mathrm{d}t} = H_\varphi\left(T_r, T_\varphi, \frac{\partial v}{\partial r}, \frac{v}{r}, \delta_r, \delta_\varphi, e\right), \tag{16}$$

$$\frac{\mathrm{d}\delta_r}{\mathrm{d}t} = F_r\left(\frac{\partial v}{\partial r}, \frac{v}{r}, \delta_r, \delta_\varphi\right), \tag{17}$$

$$\frac{\mathrm{d}\delta_\varphi}{\mathrm{d}t} = F_\varphi\left(\frac{\partial v}{\partial r}, \frac{v}{r}, \delta_r, \delta_\varphi\right), \tag{18}$$

$$\frac{\mathrm{d}e}{\mathrm{d}t} = (1+e)\left(\frac{\partial v}{\partial r} + 2\frac{v}{r}\right). \tag{19}$$

## 4. Numerical algorithm

A numerical approach developed in [10, 11] for dynamic plane-wave problems is modified here for the solution of cylindrical and spherical problems. The approach consists in the replacement of a continuous body by a discrete system with the mass of the medium being concentrated at separate surfaces (lumped masses). The equations of motion for the masses and the constitutive equations for the subdomains constitute a finite-difference approximation of the original partial differential equations.

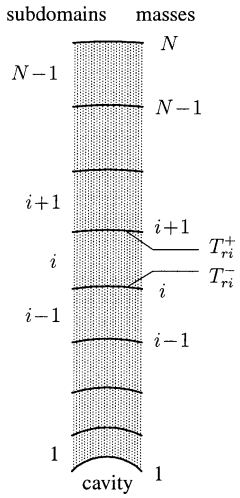


*Figure 1.* Discretisation of the domain.

### 4.1. Cylindrical problem

The domain between two concentric cylindrical surfaces of radii $r_a^0$ and $r_b^0$ where the solution is sought is divided by $N$ concentric surfaces into $N-1$ subdomains as shown in Figure 1. The mass of a subdomain $i$ is assumed to be concentrated at the surface $i$. The mass calculated per unit length in the $z$-direction and per radian in $\varphi$ is given by

$$m_i = \tfrac{1}{2}\varrho\left(r_{i+1}^2 - r_i^2\right), \tag{20}$$

where $r_i, r_{i+1}$ are the initial radii of the corresponding surfaces, and $\varrho$ stands for the initial density. The mass of the surface $N$ remains unspecified.

The equation of motion for the mass $m_i$ reads

$$\frac{m_i}{r_i}\frac{\mathrm{d}v_i}{\mathrm{d}t} = T_{ri}^{-} - T_{r(i-1)}^{+}, \tag{21}$$

where $T_{ri}^{+}, T_{ri}^{-}$ denote the stresses at the boundaries of the subdomains, see Figure 1, and $v_i$ is the radial velocity of the mass. The mass $m_i$ is independent of the change in the radius of the surface $i$ during the cavity expansion.

The stress components are assumed to vary linearly in the subdomains. If $T_{ri}$ is the value of the radial stress in the middle point of the subdomain $i$, the stresses $T_{ri}^{+}, T_{ri}^{-}$ at the boundaries are

$$T_{ri}^{+} = T_{ri} + \tfrac{1}{2}(r_{i+1} - r_i)\left.\frac{\partial T_r}{\partial r}\right|_i, \tag{22}$$

$$T_{ri}^{-} = T_{ri} - \frac{1}{2}(r_{i+1} - r_i)\left.\frac{\partial T_r}{\partial r}\right|_i. \tag{23}$$

Once the mass of the subdomains is concentrated at their boundaries, the material in the subdomains is treated as inertia-free. This allows us to find the gradient of the radial stress in (22), (23) from the static equilibrium equation

$$\frac{\partial T_r}{\partial r} + \frac{1}{r}(T_r - T_\varphi) = 0 \tag{24}$$

written for the middle of the subdomain:

$$\left.\frac{\partial T_r}{\partial r}\right|_i = 2\frac{T_{\varphi i} - T_{ri}}{r_i + r_{i+1}}. \tag{25}$$

Substitution of (22), (23), (25) in (21) gives the equation of motion of the mass $i$ in the form:

$$\frac{m_i}{r_i}\frac{\mathrm{d}v_i}{\mathrm{d}t} = T_{ri} - T_{r(i-1)} + \frac{r_{i+1} - r_i}{r_{i+1} + r_i}\left(T_{ri} - T_{\varphi i}\right) + \frac{r_i - r_{i-1}}{r_i + r_{i-1}}\left(T_{r(i-1)} - T_{\varphi(i-1)}\right). \tag{26}$$

Equation (26) is used in the numerical calculations for $i = 2$ to $N - 1$. The motion of the mass $m_1$ is determined by the equation

$$\frac{m_1}{r_1}\frac{\mathrm{d}v_1}{\mathrm{d}t} = T_{r1} + \frac{r_2 - r_1}{r_2 + r_1}\left(T_{r1} - T_{\varphi 1}\right) - T_{ra}, \tag{27}$$

where $T_{ra}$ is a boundary condition for the radial stress at $r = r_a$. The motion of the mass $m_N$ is determined by the boundary condition (13)

$$\frac{\mathrm{d}v_N}{\mathrm{d}t} = -c\frac{v_N - v_{N-1}}{r_N - r_{N-1}}. \tag{28}$$

Owing to the invariance of the masses $m_i$ with respect to the deformation of the medium, the use of the equations of motion in the form (26), (27) does not require the calculation and the updating of the density $\varrho$ in the case of large strains.

If we substitute (20) for $m_i$ in (26), we obtain

$$\frac{1}{2}\varrho\frac{r_{i+1} + r_i}{r_i}\frac{\mathrm{d}v_i}{\mathrm{d}t} = \frac{T_{ri} - T_{r(i-1)}}{r_{i+1} - r_i} + \frac{T_{ri} - T_{\varphi i}}{r_{i+1} + r_i} + \frac{(r_i - r_{i-1})\left(T_{r(i-1)} - T_{\varphi(i-1)}\right)}{(r_{i+1} - r_i)(r_i + r_{i-1})}. \tag{29}$$

It is easily seen that (29) is a finite-difference approximation of the original equation of motion (6). Equation (29) turns asymptotically into (6) as $\max\Delta r \to 0$ if

$$\lim_{\max\Delta r \to 0}\frac{r_i - r_{i-1}}{r_{i+1} - r_i} = 1. \tag{30}$$

The stress components, the intergranular-strain components and the void ratio in each subdomain are calculated by the integration of their evolution equations (8–12), (7), whereas the components of the stretching tensor are found as

$$\left.\frac{\partial v}{\partial r}\right|_i = \frac{v_{i+1} - v_i}{r_{i+1} - r_i}, \tag{31}$$

$$\left.\frac{v}{r}\right|_i = \frac{v_{i+1} + v_i}{r_{i+1} + r_i}. \tag{32}$$

The time integration of the equations is performed implicitly as

$$f(t + \Delta t) = f(t) + [\alpha f'(t) + (1 - \alpha) f'(t + \Delta t)]\Delta t, \tag{33}$$

where $f$ and $f'$ denote the set of the unknown functions and their time derivatives, respectively, and $\alpha$ is the parameter of the scheme, $0 \leqslant \alpha < 1$. Equation (33) is solved by successive approximations.

### 4.2. Spherical problem

The numerical scheme for the spherical problem can be constructed in a similar way. Omitting intermediate computations, we write out only equations corresponding to (20), (26), (27):

$$m_i = \frac{1}{3}\varrho\left(r_{i+1}^3 - r_i^3\right), \tag{34}$$

$$\frac{m_i}{r_i^2}\frac{\mathrm{d}v_i}{\mathrm{d}t} = T_{ri} - T_{r(i-1)} + 2\frac{r_{i+1}-r_i}{r_{i+1}+r_i}(T_{ri} - T_{\varphi i}) + 2\frac{r_i - r_{i-1}}{r_i + r_{i-1}}\left(T_{r(i-1)} - T_{\varphi(i-1)}\right), \tag{35}$$

$$\frac{m_1}{r_1^2}\frac{\mathrm{d}v_1}{\mathrm{d}t} = T_{r1} + 2\frac{r_2 - r_1}{r_2 + r_1}(T_{r1} - T_{\varphi 1}) - T_{ra}. \tag{36}$$

## 5. Numerical examples

Numerical solutions presented below are calculated for a cylindrical cavity with an initial radius of 0·2 m, with a homogeneous initial stress state $T_r = T_\varphi = T_z = -100$ kPa and an initial void ratio of 0·9. For dry sand this void ratio corresponds to an initial density of $1{\cdot}4 \times 10^3$ kg/m$^3$. The outer boundary of the computational domain is taken at $r_b^0 = 30$ m.

To show the numerical performance of the boundary condition (13), let the cavity be loaded by a single pressure impulse on the cavity wall as shown in Figure 2. Two cases of the boundary condition at the outer boundary are considered: the case $T_r = \text{const} = -100$ kPa and the transparent boundary condition (13). The corresponding solutions are compared in Figure 3. It is seen that the inaccuracy related to the boundary condition (13) caused by the cylindrical geometry, the non-elastic effects in the material behaviour and by the numerics itself is negligible: the outgoing wave goes through the boundary without reflection.

In the further examples, the cavity is loaded by a cyclic sinusoidal pressure $T_r$ on the cavity wall varying between $-100$ and $-150$ kPa. Figures 4–7 show two cases with different frequencies, 30 and 10 Hz, with all other parameters being the same as before.

The periodic loading results in a steady increase of the cavity radius. Figure 4 shows the change in the radius during the first 30 cycles of the loading. In spite of the fact that the amplitude of the loading is the same in both cases, the rate of expansion (the change in the radius per cycle) in the high-frequency case of 30 Hz is 60 times higher than in the low-frequency case of 10 Hz.

The dynamic pressure-expansion curves at the beginning of the expansion are compared in Figure 5. The curves are essentially different. The hysteresis and, consequently, the work done by the loading in one cycle is much higher in the high-frequency case.

The cyclic loading of the cavity is accompanied by cyclically changing shear stresses in the vicinity of the cavity. According to the general characteristics of granular materials, this

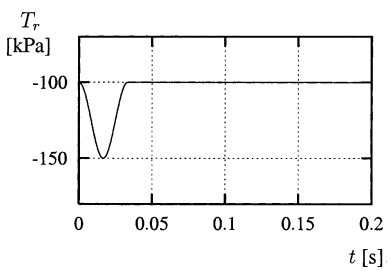


*Figure 2.* Boundary condition at $r_a = 0{\cdot}2$ m for the solutions shown in Figure 3.

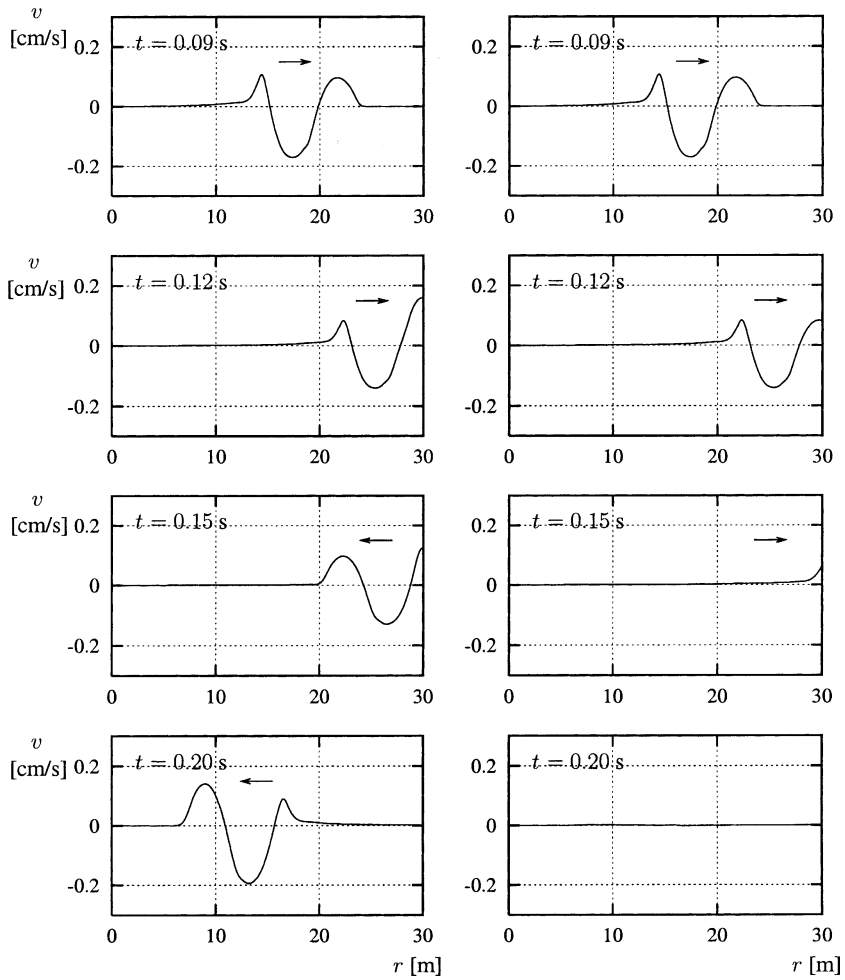


*Figure 3.* Velocity profiles at different times produced by a pressure impulse (Figure 2) in a cylindrical cavity with $r_a^0 = 0{\cdot}2$ m. Left column: boundary condition $T_r = \text{const}$ at $r_b = 30$ m. Right column: the nonreflecting plane-wave boundary condition (13) at $r_b = 30$ m.

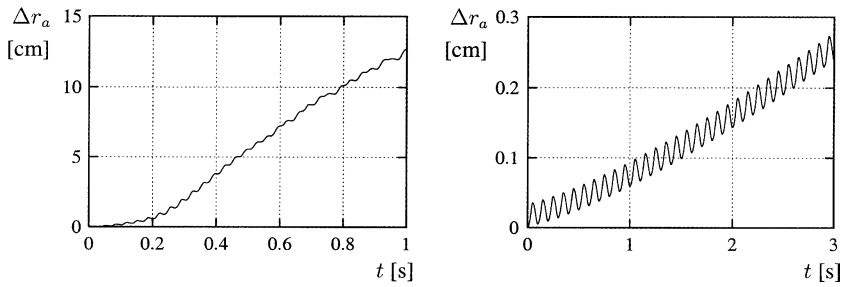


*Figure 4.* The change in the radius of a cylindrical cavity loaded by a cyclic pressure varying between $-100$ and $-150$ kPa with a frequency of 30 Hz (left) and 10 Hz (right). Initial radius: 0·2 m.

results in a gradual compaction of the material. The change in the void ratio in the vicinity of the cavity is shown in Figure 6 which again reveals a pronounced influence of the frequency on the solution. Not only is the rate of compaction much higher in the high-frequency case, but also the compaction spreads much farther from the cavity wall. Obviously,

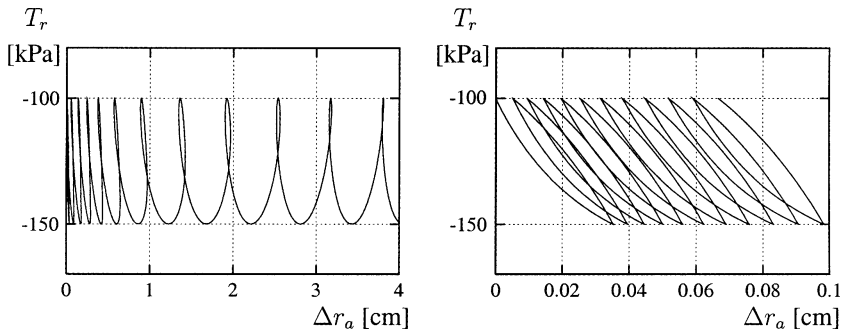


*Figure 5.* Pressure-expansion curves for the same problems as in Figure 4. Left: 30 Hz, right: 10 Hz.

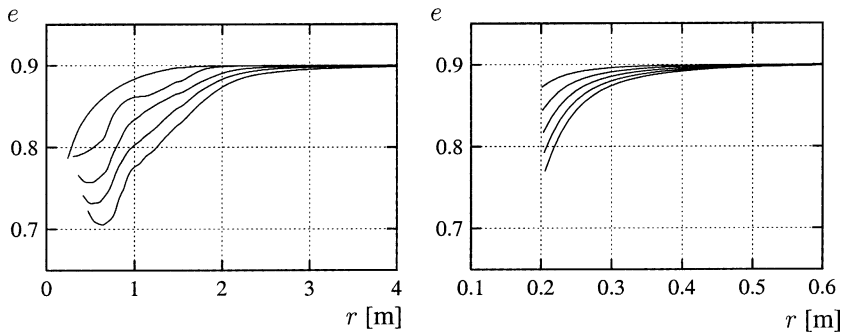


*Figure 6.* Void ratio in the vicinity of the cavity after 12, 24, 36, 48 and 60 cycles of loading (from the upper to the lower curve, respectively). Left: 30 Hz, right: 10 Hz.

in cavity problems the compaction of the material facilitates the increase of the cavity radius as compared to problems in which the material does not exhibit steady compaction or is incompressible.

The cavity expansion not only leads to the compaction of the material in the vicinity of the cavity but also to the change in the stress state. The time dependence of the stress components in the material element initially situated at $r = 1{\cdot}0$ m is shown in Figure 7. In the high-frequency case, the average absolute values of all stress components are rapidly reduced at the beginning of the loading and then change rather slowly. The ratios between the average values after the reduction do not correspond to a hydrostatic state as was the case initially. In the low-frequency case, apart from the fact that the average values of the stresses change slowly, the amplitudes of the stresses are much smaller.

The significant reduction in the stress level observed in the high-frequency case can be explained if we again recall that, according to the general characteristics of granular materials, cyclic shearing leads to compaction or, if volume change is prohibited by kinematical restrictions, to a reduction in the pressure. Although the material in the vicinity of the cavity is compacted due to the cyclic deformation, this compaction is not enough for the mean pressure to remain at the same level. As a result, the absolute values of the stresses decrease.

As mentioned in the Introduction, the change in the stress amplitudes with radius is different in the quasi-static and the dynamic problems: the stresses decrease slower in the dynamic case and thus spread farther from the cavity. For a cylindrical cavity in an elastic medium, the stress amplitudes are proportional to $1/r^n$ (in the dynamic case – asymptotically for $r \to \infty$) with $n = 2$ and $0{\cdot}5$ for the quasi-static and the dynamic problems, respectively. For the two numerical examples just considered, Table 1 shows the amplitudes of the stress component $T_r$

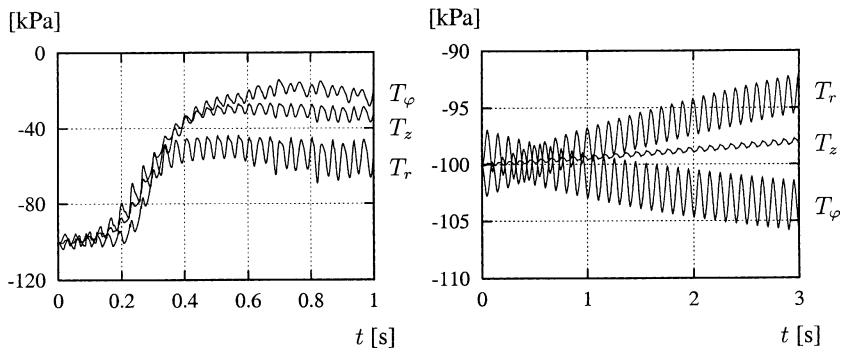


*Figure 7.* Stress components at $r = 1{\cdot}0$ m versus time. Left: 30 Hz, right: 10 Hz.

*Table 1.* Comparison of the solutions.

| Frequency (Hz) | $\Delta T_r(r_a)$ (kPa) | $\Delta T_r(r)$ (kPa) | $n$ (37) |
|---|---|---|---|
| 30 | 50 | 12–20 | 0·75–1·0 |
| 10 | 50 | 2·9 | 1·77 |
| 30 | 1 | 0·056 | 1·79 |

at two points with initial coordinates $r_a = 0{\cdot}2$ m (cavity wall) and $r = 1$ m. In the first example (30 Hz) the stress amplitude at $r = 1$ m is taken for $t > 0{\cdot}5$ s. The exponent $n$ given in Table 1 is estimated from the stress amplitudes at the two points by the formula

$$n = \frac{\log[\Delta T_r(r)/\Delta T_r(r_a)]}{\log(r_a/r)}. \tag{37}$$

The exponent $n$ for the low-frequency problem is greater and closer to that for the quasi-static solution. Also shown in Table 1 is a third case for a frequency of 30 Hz and a small loading amplitude of 1 kPa. Surprisingly, despite the high frequency, the attenuation of the stresses in this case is high and results in a high exponent $n$. The explanation is, however, simple: the small-amplitude loading causes nearly elastic deformations which are characterised by relatively high stiffness and, correspondingly, by a large wavelength. In this case the speed of longitudinal small-amplitude waves, which is estimated from the constitutive equation, is about 260 m/s, which for a frequency of 30 Hz gives a wavelength of 8·7 m – large enough in comparison with the cavity size. Contrary to this, the plastic deformations which the material undergoes during large-amplitude loading are characterised by lower stiffness and shorter wavelengths.

Solutions to the spherical problem are qualitatively similar to those to the cylindrical problem: the expansion is also accompanied by the compaction of the material and by the decrease in the absolute values of stresses in the vicinity of the cavity. There are, however, noticeable quantitative differences: if the spherical problem is solved with the same parameters, the attenuation of the stress amplitude with distance from the cavity is much higher than in the cylindrical case. As a consequence, the rate of the cavity expansion and the rates of the compaction and the stress reduction are much lower.

## 6. Discussion of applications

The cavity-expansion problem described above allows us to model dynamic processes related to the cyclic deformation of granular soils such as deep vibratory compaction [8] (cylindrical cavity) and vibratory pile driving (spherical cavity).

In the deep vibratory compaction technique, the soil is compacted by a vibrating steel cylinder (vibrator) placed vertically in a soil layer. The vibrator is 30–45 cm in diameter, 3–5 m in length and has inside a motor with a rotating eccentric mass which causes the axis of the vibrator to rotate about the vertical axis with a frequency of 30–60 Hz.

The accurate modelling of deep vibratory compaction is extremely difficult if at all possible (in this connection we refer to [18]). This is not only because of the complicated material behaviour but also due to the fact that the dynamic problem describing the deformation of the soil surrounding the vibrator is spatially three-dimensional. Additional difficulties arise when taking into account the inflow of the new material from above to the immediate vicinity of the vibrator.

The main goal in the modelling of deep vibratory compaction is to reveal the dependence of the compaction on the parameters of the vibrator and the soil in order to optimise the process. The solution of two- or three-dimensional problems is time-consuming and can therefore hardly serve this purpose. The one-dimensional problem considered in this paper involves much less computing time and can thus provide much data required for a detailed modelling.

The two main simplifications entailed in the reduction of the deep vibratory compaction problem to a one-dimensional one consist in the fact that the rotating force produced by the vibrator is replaced with an axially symmetric loading, and that the contribution of the vertical displacement of the soil to the compaction is not taken into account. In order to assess the influence of these simplifications, a number of solutions to the one-dimensional problem should be compared with the corresponding solutions to a two- or three-dimensional problem. This may result in establishing correction factors which could subsequently be used in a one-dimensional analysis.

The introduction of correction factors, either by comparison with experimental data or with more sophisticated numerical calculations, is also necessary when applying the dynamic cavity-expansion theory to the modelling of vibratory pile driving. For the quasi-static penetration this approach was adopted, for instance, in [19].

## Appendix. Constitutive functions

The tensors $\mathcal{L}$ and N in (1), (2) are written as [9]

$$\mathcal{L}_{ijkl} = \frac{f_b f_e}{\mathrm{tr}(\hat{\mathrm{T}}^2)}[F^2 \delta^K_{ik}\delta^K_{jl} + a^2 \hat{T}_{ij}\hat{T}_{kl}], \tag{A.1}$$

$$N_{ij} = \frac{f_b f_e f_d a F}{\mathrm{tr}(\hat{\mathrm{T}}^2)}(\hat{T}_{ij} + \hat{T}^*_{ij}), \tag{A.2}$$

where $\delta^K_{ij}$ is the Kronecker delta, and

$$\hat{T}_{ij} = \frac{T_{ij}}{\mathrm{trT}}, \qquad \hat{T}^*_{ij} = \hat{T}_{ij} - \tfrac{1}{3}\delta^K_{ij}. \tag{A.3}$$

The factor $a$ in (A1), (A2) is determined by the friction angle $\varphi_c$ in critical states:

$$a = \sqrt{\frac{3}{8}}\frac{(3 - \sin\varphi_c)}{\sin\varphi_c}. \tag{A.4}$$

The factor $F$ is a function of $\hat{\mathbf{T}}^*$:

$$F=\sqrt{\frac{1}{8}\tan^2\xi+\frac{2-\tan^2\xi}{2+\sqrt{2}\tan\xi\cos 3\theta}}-\frac{1}{2\sqrt{2}}\tan\xi, \tag{A.5}$$

where

$$\tan\xi=\sqrt{3}\|\hat{\mathbf{T}}^*\|,\quad \cos 3\theta=-\sqrt{6}\frac{\mathrm{tr}(\hat{\mathbf{T}}^{*3})}{[\mathrm{tr}(\hat{\mathbf{T}}^{*2})]^{3/2}}. \tag{A.6}$$

The factors $a$ and $F$ determine the critical-state surface in the stress space.

Three characteristic void ratios are specified as functions of the mean pressure: the minimal possible void ratio, $e_d$, the critical void ratio, $e_c$, and the void ratio in the loosest state, $e_i$. The pressure dependence of these void ratios is postulated in the form (compressive stresses are negative)

$$\frac{e_i}{e_{i0}}=\frac{e_c}{e_{c0}}=\frac{e_d}{e_{d0}}=\exp\left[-\left(\frac{-\mathrm{tr}\mathbf{T}}{h_s}\right)^n\right], \tag{A.7}$$

with the corresponding reference values $e_{i0}, e_{c0}, e_{d0}$ for zero pressure ($e_{i0}>e_{c0}>e_{d0}$). The constants $e_{i0}, e_{c0}, e_{d0}$ with the $h_s, n$ are material parameters.

The factor

$$f_d=\left(\frac{e-e_d}{e_c-e_d}\right)^\alpha, \tag{A.8}$$

where $\alpha$ is a material parameter, tends to unity as the state of the material approaches a critical state. The functions $f_e$ and $f_b$ are defined as

$$\begin{aligned} f_e&=\left(\frac{e_c}{e}\right)^\beta,\\ f_b&=\frac{h_s}{n}\left(\frac{1+e_i}{e_i}\right)\left(\frac{e_{i0}}{e_{c0}}\right)^\beta\left(\frac{-\mathrm{tr}\mathbf{T}}{h_s}\right)^{1-n}\left[3+a^2-\sqrt{3}a\left(\frac{e_{i0}-e_{d0}}{e_{c0}-e_{d0}}\right)^\alpha\right]^{-1}, \end{aligned} \tag{A.9}$$

with a parameter $\beta$.

The tensor $\mathcal{M}$ in (2) is written as

$$\begin{aligned} \mathcal{M}_{ijkl}=&[\rho^\chi m_T+(1-\rho^\chi)m_R]\mathcal{L}_{ijkl}\\ &+\begin{cases}\rho^\chi(1-m_T)\mathcal{L}_{ijqs}\hat{\delta}_{qs}\hat{\delta}_{kl}+\rho^\chi N_{ij}\hat{\delta}_{kl} & \text{if } \hat{\delta}_{ij}D_{ij}>0,\\ \rho^\chi(m_R-m_T)\mathcal{L}_{ijqs}\hat{\delta}_{qs}\hat{\delta}_{kl} & \text{if } \hat{\delta}_{ij}D_{ij}\leqslant 0,\end{cases} \end{aligned} \tag{A.10}$$

where

$$\hat{\delta}_{ij}=\begin{cases}\delta_{ij}/\|\boldsymbol{\delta}\| & \text{if } \boldsymbol{\delta}\neq\mathbf{0},\\ 0 & \text{if } \boldsymbol{\delta}=\mathbf{0},\end{cases} \tag{A.11}$$

$\rho=\|\boldsymbol{\delta}\|/R$, and $R, m_R, m_T, \chi$ are constitutive parameters.

The evolution equation (3) for the intergranular-strain tensor $\boldsymbol{\delta}$ is written as

$$\frac{\mathrm{d}\delta_{ij}}{\mathrm{d}t}=\begin{cases}D_{ij}-\rho^{\beta_r}\hat{\delta}_{ij}\hat{\delta}_{kl}D_{kl} & \text{if } \hat{\delta}_{ij}D_{ij}>0,\\ D_{ij} & \text{if } \hat{\delta}_{ij}D_{ij}\leqslant 0\end{cases} \tag{A.12}$$

with a parameter $\beta_r$.

The constitutive parameters used in the numerical examples in this paper are given in Table 2.

*Table 2.* Constitutive parameters.

| $\varphi_c[^\circ]$ | $h_s$[MPa] | $e_{c0}$ | $e_{d0}$ | $e_{i0}$ | $\alpha$ | $\beta$ | $n$ | $R$ | $m_R$ | $m_T$ | $\beta_r$ | $\chi$ |
|---|---|---|---|---|---|---|---|---|---|---|---|---|
| 33 | 1000 | 0·95 | 0·55 | 1·05 | 0·25 | 1·5 | 0·25 | $4 \times 10^{-5}$ | 5·0 | 5·0 | 0·05 | 1·5 |

## Acknowledgements

The present study was initiated within the framework of SFB 298 financed by the Deutsche Forschungsgemeinschaft. The study has also been supported by the Stiftung für geotechnische Grundlagenforschung, Universität für Bodenkultur Wien.

## References

1. H.S. Yu, *Cavity Expansion Methods in Geomechanics*. Dordrecht: Kluwer (2000) 404 pp.
2. A.S. Vesić, Expansion of cavities in infinite soil mass *ASCE J. Soil Mech. Found. Div.* 98 (1972) 265–290.
3. J.P. Carter, J.R. Booker and S.K. Yeung, Cavity expansion in cohesive frictional soils. *Géotechnique* 36 (1986) 349–358.
4. H.S. Yu and G.T. Houlsby, Finite cavity expansion in dilatant soils: loading analysis. *Géotechnique* 41 (1991) 173–183.
5. I. Collins, M. Pender and W. Yan, Cavity expansion in sands under drained loading conditions. *Int. J. Num. Anal. Meth. Geomech.* 16 (1992) 3–23.
6. D. Shuttle and M. Jefferies, Dimensionless and unbiased CPT interpretation in sand. *Int. J. Num. Anal. Meth. Geomech.* 22 (1998) 351–391.
7. V.A. Osinov and R. Cudmani, Theoretical investigation of the cavity expansion problem based on a hypoplasticity model. *Int. J. Num. Anal. Meth. Geomech.* 25 (2001) 473–495.
8. R.E. Brown, Vibroflotation compaction of cohesionless soils. *ASCE J. Geotech. Eng. Div.* 103 (1977) 1437–1451.
9. A. Niemunis and I. Herle, Hypoplastic model for cohesionless soils with elastic strain range. *Mech. Cohesive-frictional Mater*. 2(4) (1997) 279–299.
10. V.A. Osinov, Wave-induced liquefaction of a saturated sand layer. *Cont. Mech. Thermodyn*. 12 (2000) 325–339.
11. V.A. Osinov, A numerical model for the site response analysis and liquefaction of soil during earthquakes. In: O. Natau, E. Fecker and E. Pimentel (eds.), *Geotechnical Measurements and Modelling*. Lisse: Swets & Zeitlinger (2003) pp. 475–481.
12. V.A. Osinov and G. Gudehus. Dynamics of hypoplastic materials: theory and numerical implementation. In: K. Hutter and N. Kirchner (eds.), *Dynamic Response of Granular and Porous Materials under Large and Catastrophic Deformations*. Berlin: Springer (2003) pp. 265–284.
13. J.M. Hill, Some symmetrical cavity problems for a hypoplastic granular material. *Quart. J. Mech. Appl. Math*. 53 (2000) 111–135.
14. G. Gudehus, A comprehensive constitutive equation for granular materials. *Soils and Foundations* 36 (1996) l–12.
15. P.A. von Wolffersdorff, A hypoplastic relation for granular materials with a predefined limit state surface. *Mech. Cohesive-frictional Mater*. 1 (1996) 251–271.
16. E. Bauer and W. Wu, A hypoplastic model for granular soils under cyclic loading. In: D. Kolymbas (ed.), *Modern Approaches to Plasticity*. Amsterdam: Elsevier (1993) pp. 247–258.
17. A. Niemunis, Hypoplasticity vs. elastoplasticity, selected topics. In: D. Kolymbas (ed.), *Modern Approaches to Plasticity*. Amsterdam: Elsevier (1993) pp. 277–307.
18. W. Fellin, *Rütteldruckverdichtung als plastodynamisches Problem*. Rotterdam: Balkema (2000) 94 pp.
19. R. Cudmani and V.A. Osinov, The cavity expansion problem for the interpretation of cone penetration and pressuremeter tests. *Canadian Geot. J*. 38 (2001) 622–638.